Karlsruhe Institute of Technology

Interpretation of decreasing peak-shift for Raman-peaks in silica

K. Günter Schell, Claudia Bucharsky,
Susanne Wagner, Theo Fett

KIT SCIENTIFIC WORKING PAPERS 254

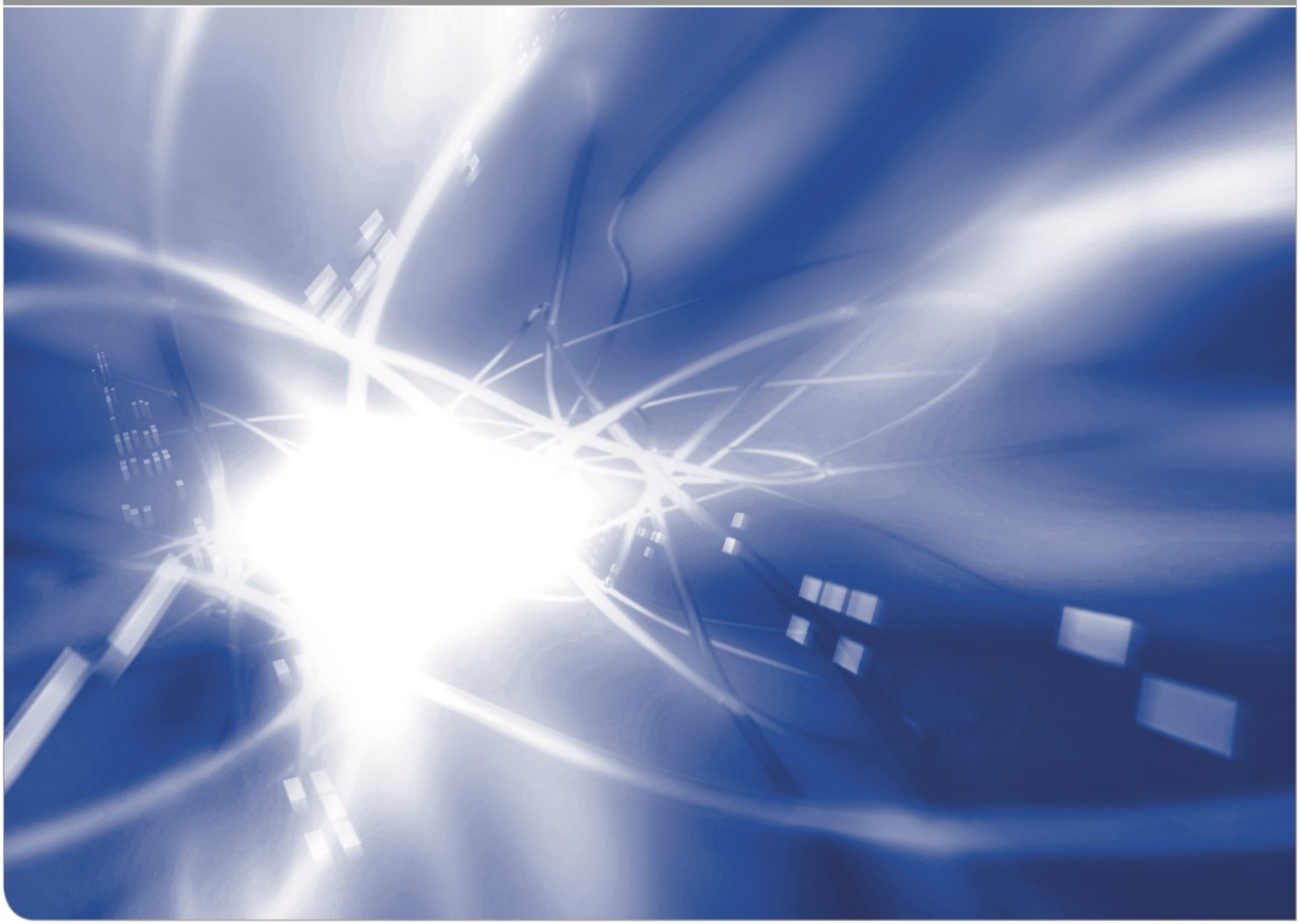

Institute for Applied Materials

Impressum

Karlsruher Institut für Technologie (KIT)
www.kit.edu

2024

ISSN: 2194-1629

Abstract

A first interpretation of the influence of stress on the IR- and the Raman-peak frequencies was made possible via its influence on the binding angles. The stress effect was assumed as a consequence of a change of the bond angles due to the stresses.

In addition we could show that the angle stretching is not necessarily the only effect that influences the position of the frequency of IR lines. We addressed the change in the peak position under uniaxial tension and compression in computations using the Lennard-Jones potential.

From our computations, we have to expect decreasing frequency under tension and increasing frequency under compression loading. In our opinion, this contribution of frequency shift has to be added to the contribution by the angle stretching.

Contents

1. On the position of Raman-maxima under stresses

1.1 Experimental results from literature

The interpretation of stress influences on the position of IR- and Raman-lines that has been dominant to date is based on Galeener's [1] suggestion. In our opinion, other effects are also possible that can also influence the position of the lines in the IR spectrum or the Raman spectrum. An example for the influence of stresses are measurements under uniaxial tensile stresses by Tallant et al. [2], shown in Fig. 1 (“Frequency” in terms of the wavenumber). In this diagram, the highest two vibration bands are plotted with colored symbols and denoted in the nomenclature of Sen and Thorpe [3] and Galeener [1] by the numbers (1)-(4).

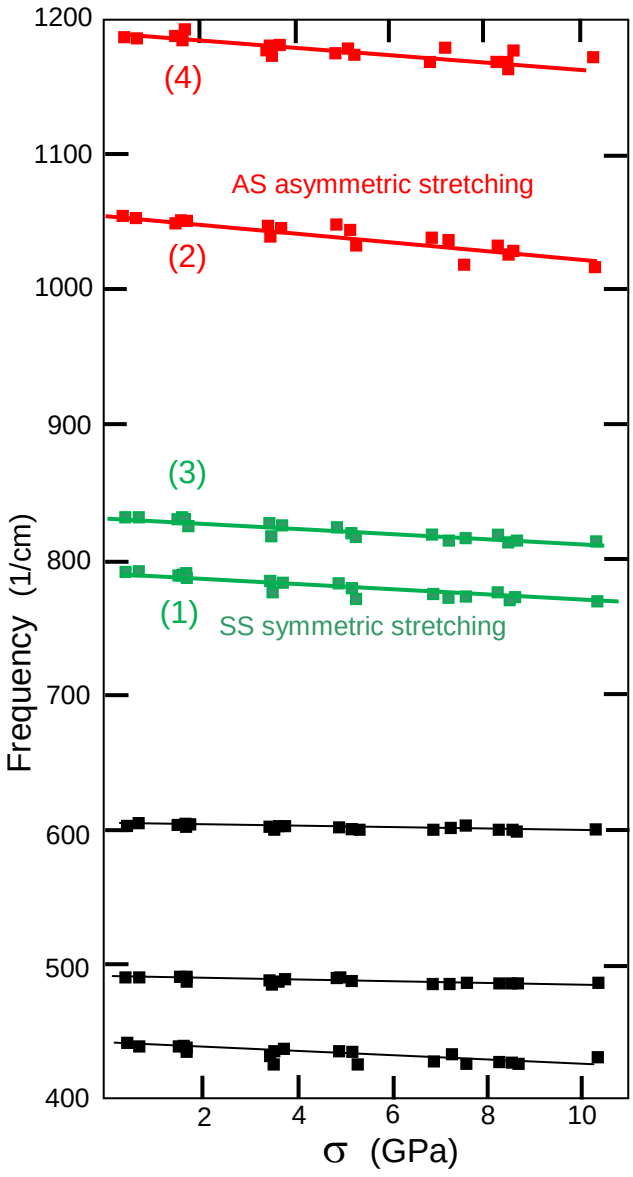

Fig. 1 Measurements by Tallant et al [2] on silica by tensile tests, numbers in parentheses correspond to eqs.(1)-(4).

Figure 2 compiles the peak-position as a function of the hydrostatic stress according to data from [4] obtained from measurements by Tallant et al. [2], Hemley et al. [5], Vandembroucq et al. [6], Deschamps et al. [7], and Tomozawa et al. [8].

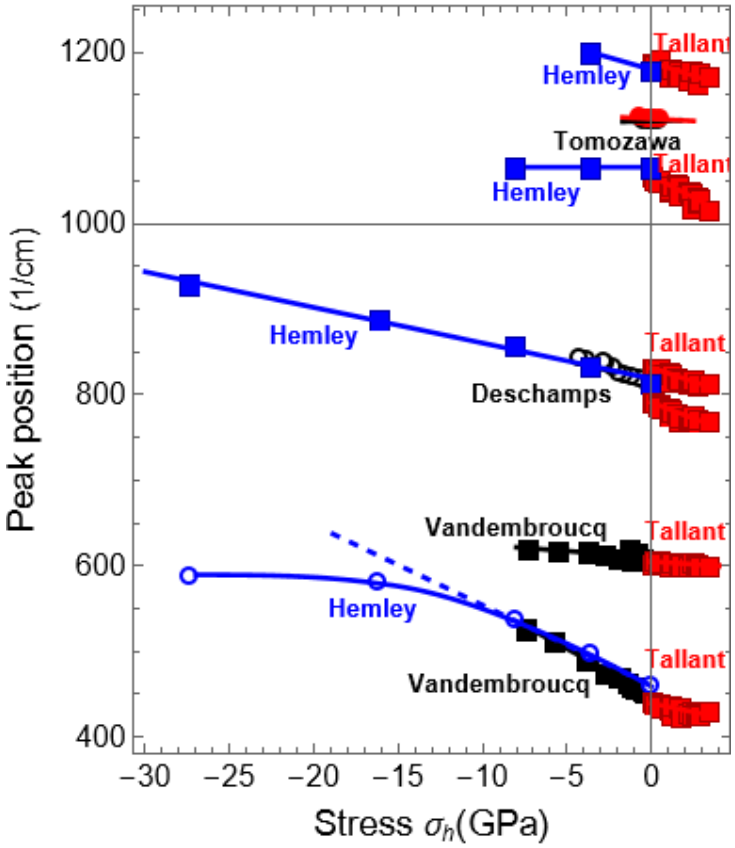

Fig. 2 Stress-dependent peak positions as a function of the *hydrostatic stress component* σ_h.

1.2 Galeener's solution

The infrared spectrum for silica glass shows a shifting of infrared peaks under stresses. The strongness and direction of the peak shift depends on the chosen IR-peak frequency and the surface state (water-affected, annealed, etched [8]). A first interpretation of the influence of stress on the IR frequency was made possible by its influence on the bond angles, as had been shown very early by Galeener [1].

Galleener suggested for the dependency between the angular frequency ω and the bond angle θ for the special case of the antisymmetric and the symmetric stretching modes [1, 3]

$$\omega_1^2 = (\alpha / m_O)(1 + \cos\theta) \tag{1}$$

$$\omega_2^2 = (\alpha / m_O)(1 - \cos\theta) \tag{2}$$

$$\omega_3^2 = \omega_1^2 + (4\alpha / 3m_A) \tag{3}$$

$$\omega_4^2 = \omega_2^2 + (4\alpha / 3m_A) \tag{4}$$

where m_O =16 is the atomic mass of the oxygen atom, m_A =28 the atomic mass of the silicon atom, and α a bond-stretching parameter. The parameters α as well as θ can depend on the global stress state, i.e. α=α(σ) and θ=θ(σ). In the absence of stresses, the bond angle is θ_0, and given by $\theta_0 \cong 130° = 13/18 \times \pi$ as can be concluded from Fig. 3. This plot compiles literature results for the peak position as a function of the bridging angle from Devine [9] and Tomozawa [10].

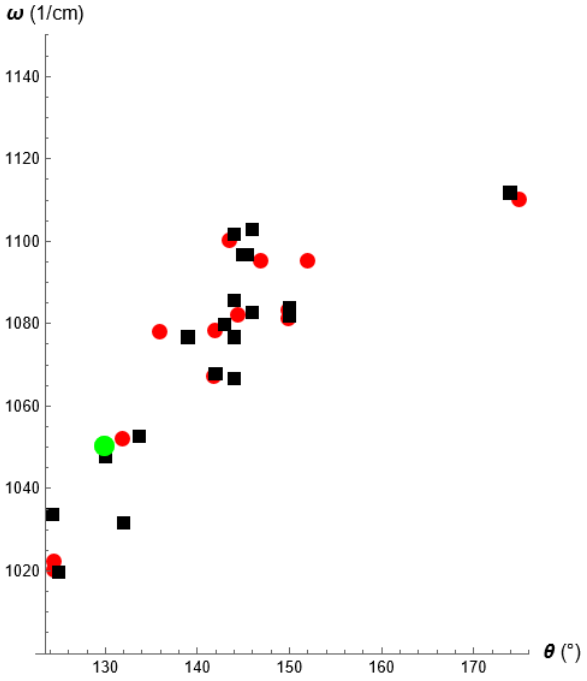

Fig. 3 Literature results for peak positions (in cm^{-1}) as a function of the bridging bond angle θ_0. Squares: measurements compiled by Devine [9], red circles: values reported by Tomozawa [10], green circle: Data point for θ_0=130° and ω=1050/cm.

The frequencies in the absence of stresses are

$$\begin{aligned} \omega_{1,0}^2 &= (\alpha / m_O)(1 - \sin[2\pi / 9]) \\ &\cong 0.3572\,(\alpha / m_O) \end{aligned} \tag{5}$$

$$\begin{aligned} \omega_{2,0}^2 &= (\alpha / m_O)(1 + \sin[2\pi / 9]) \\ &\cong 1.6428\,(\alpha / m_O) \end{aligned} \tag{6}$$

$$\omega_{3,0}^2 = \omega_{1,0}^2 + (4\alpha / 3m_A) \tag{7}$$

$$\omega_{4,0}^2 = \omega_{2,0}^2 + (4\alpha / 3m_A) \tag{8}$$

Figure 4 illustrates the equations (1-4) in normalized representation.

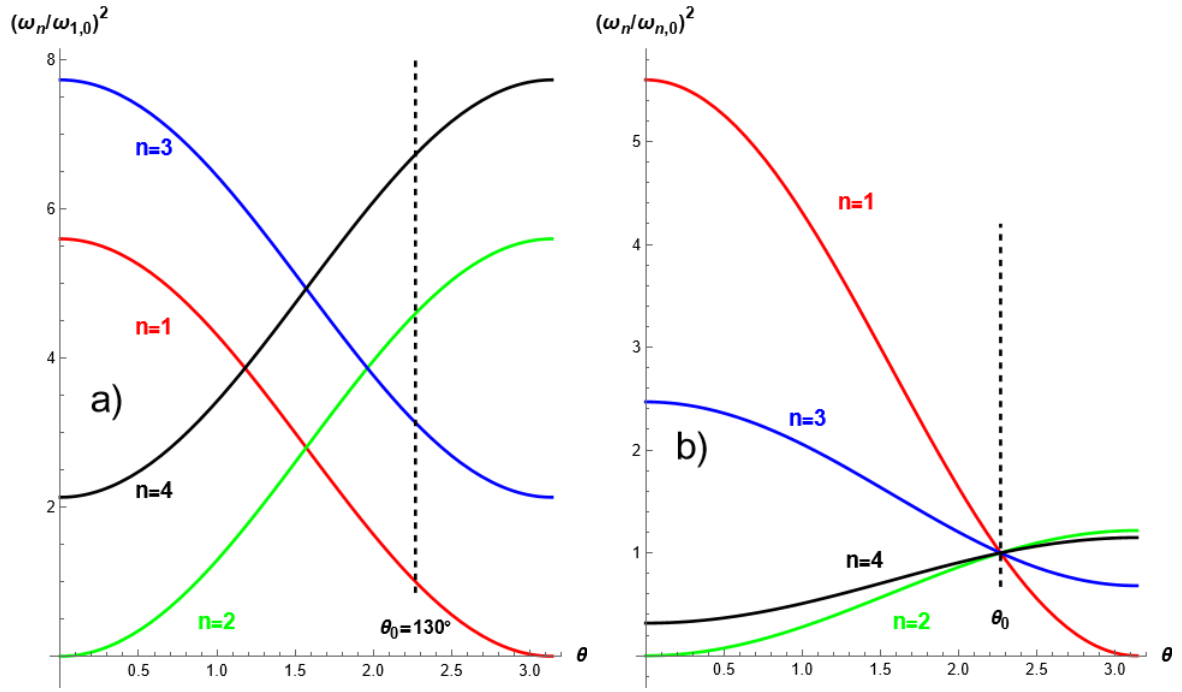

Fig. 4 Peak heights as a function of the angle θ, a) normalization on the value for n=1 and $\theta=\theta_0$; b) normalization on the individual peak positions in the absence of stresses; dashed perpendicular line shows the angle $\theta_0 \cong 130°$.

In Fig. 4, the squares of the peak position are plotted versus the angle θ in rad. In Fig. 4a the peak position is normalized on the peak position in the absence of stresses. The numbers at the curves indicate the number of the related equation. The dashed perpendicular line shows the angle θ_0, which is about 130° for SiO_2. Figure 4b illustrates the same results but normalized on the individual peak positions for each value *n*=1-4. It is trivial that in this representation all curves must cross at θ_0.

As Tomozawa et al. [8,10] argued, the equilibrium angle θ should increase under tensile stress, i.e.

$$d\theta / d\sigma \geq 0 \tag{9}$$

Under this condition, decreasing peak positions for n=1 and n=3 and increasing ones for n=2 and n=4 would be expected for tensile stresses. However, such behavior is not observed in the experiments.

2. Effect of stress on binding potential

2.1 Results from Schell et al.

In [11], we showed that the effect of angle stretching by a tensile stress according to eq.(9) is not the only effect that influences the position of the frequency of IR lines. Based on the Lennard-Jones potential, we were able to derive a relationship for the change in the frequency of the IR or Raman lines as a function of the mechanical stress.

When k denotes the "spring constant" under the applied stress σ_{appl}, k_0 the spring constant in the absence of stresses and σ_{th} the theoretical strength (the strength in the absence of any crack), we derived in [11] the following linear approximation up to an applied stress of around $\sigma_{appl}/\sigma_0=0.4$:

$$\frac{k}{k_0} \cong 1 - \frac{147}{169}\left(\frac{7}{13}\right)^{1/6} \frac{\sigma_{appl}}{\sigma_{th}} \tag{10}$$

Since k represents the same mechanical binding behavior as the parameter α in eqs.(1) -(8), it trivially holds

$$\frac{k}{k_0} = \frac{\alpha}{\alpha_0} \tag{11}$$

The minus sign in eq.(10) indicates that the tensile stress applied to the bond must always lead to a decrease of the vibration frequency ω with increasing stress. This is a consequence of

$$\omega \propto \sqrt{\frac{k}{k_0}} \Rightarrow \frac{\omega}{\omega_0} \cong 1 - \frac{147}{338}\left(\frac{7}{13}\right)^{1/6} \frac{\sigma_{appl}}{\sigma_{th}} \tag{12}$$

In the following considerations, we should distinguish between the strength of a single bond and that of an undamaged body. In a previous study [4], we had calculated the maximum force transmitted by a bond, F_{max}. Under the implicit simplification that all bonds are oriented in the longitudinal direction (the x-direction), the theoretical strength of the single bond is here denoted as σ_{th}.

In the case of a statistically random bond arrangement, only 1/3 of all the bonds will be oriented in the longitudinal direction and thus only 1/3 of the longitudinal forces F_{max} contribute to the uniaxial strength. The ideal strength σ_0 of the undamaged glass sample will then be 1/3 of the considered theoretical strength of the three-dimensional arrangement, namely $\sigma_0=1/3\ \sigma_{th}$.

2.2 Superposition of the individual effects

From eq.(9) and (12) we can see, that the effect of stresses on the binding angle θ and the spring constant k must show *opposite effects* on the sign of the frequency change.
The total change of the peak position can be calculated for small changes in ω and under the condition $\theta \neq f(k)$ via the total differential

$$\mathrm{d}\omega^2 = \left(\frac{\partial\omega^2}{\partial k}\right)_{k_0} \mathrm{d}k + \left(\frac{\partial\omega^2}{\partial\theta}\right)_{\theta_0} \mathrm{d}\theta$$

$$\frac{\mathrm{d}(\omega/\omega_0)^2}{\mathrm{d}\sigma} = \left(\frac{\partial(\omega/\omega_0)^2}{\partial k}\right)_{k_0} \underbrace{\frac{\mathrm{d}k}{\mathrm{d}\sigma}}_{<0} + \left(\frac{\partial(\omega/\omega_0)^2}{\partial\theta}\right)_{\theta_0} \underbrace{\frac{\mathrm{d}\theta}{\mathrm{d}\sigma}}_{\geq 0} \tag{13}$$

By using eqs.(1)-(4) with eqs.(11) and (12), the partial differentials in eq.(13) can be evaluated. The result is in terms of coefficients c_{11}-c_{42}, where the first index denotes the numbers of the Galeener notation. The second coefficient stands for the first and second partial derivations in (13)

$$\frac{\mathrm{d}(\omega_n/\omega_{n,0})^2}{\mathrm{d}\sigma} = c_{n1}\frac{\mathrm{d}k}{\mathrm{d}\sigma} + c_{n2}\frac{\mathrm{d}\theta}{\mathrm{d}\sigma} \tag{14}$$

where
$$c_{n1} = \left(\frac{\partial(\omega_n/\omega_{n,0})^2}{\partial k}\right)_{k_0}, \quad c_{n2} = \left(\frac{\partial(\omega_n/\omega_{n,0})^2}{\partial\theta}\right)_{\theta_0} \tag{15}$$

$$\begin{aligned} c_{11} &= \left(\frac{\partial(\omega_1/\omega_{1,0})^2}{\partial k}\right)_{k_0} = \frac{1}{k_0}, \\ c_{12} &= \left(\frac{\partial(\omega_1/\omega_{1,0})^2}{\partial\theta}\right)_{\theta_0} = -\frac{\cos[2\pi/9]}{1-\sin[2\pi/9]} \cong -2.14 \end{aligned} \tag{16}$$

$$\begin{aligned} c_{21} &= \left(\frac{\partial(\omega_2/\omega_{2,0})^2}{\partial k}\right)_{k_0} = \frac{1}{k_0}, \\ c_{22} &= \left(\frac{\partial(\omega_2/\omega_{2,0})^2}{\partial\theta}\right)_{\theta_0} = \frac{\cos[2\pi/9]}{1+\sin[2\pi/9]} \cong 0.466 \end{aligned} \tag{17}$$

and with m_O=16, m_A=28:

$$\begin{aligned} c_{31} &= \left(\frac{\partial(\omega_3/\omega_{3,0})^2}{\partial k}\right)_{k_0} = \frac{1}{k_0}, \\ c_{32} &= \left(\frac{\partial(\omega_3/\omega_{3,0})^2}{\partial\theta}\right)_{\theta_0} = -\frac{\cos[2\pi/9]}{\frac{37}{21}-\sin[2\pi/9])} \cong -0.684 \end{aligned} \tag{18}$$

$$c_{41} = \left(\frac{\partial(\omega_4 / \omega_{4,0})^2}{\partial k} \right)_{k_0} = \frac{1}{k_0}, \qquad c_{42} = \left(\frac{\partial(\omega_4 / \omega_{4,0})^2}{\partial \theta} \right)_{\theta_0} = \frac{\cos[2\pi/9]}{\frac{37}{21} + \sin[2\pi/9]} \cong 0.3185 \tag{19}$$

Now eq.(14) can be written

for n=1
$$\frac{\mathrm{d}(\omega_1 / \omega_{1,0})^2}{\mathrm{d}\sigma} = \frac{1}{k_0}\frac{\mathrm{d}k}{\mathrm{d}\sigma} - 2.14\frac{\mathrm{d}\theta}{\mathrm{d}\sigma} < 0 \tag{20}$$

for n=2
$$\frac{\mathrm{d}(\omega_2 / \omega_{2,0})^2}{\mathrm{d}\sigma} = \frac{1}{k_0}\frac{\mathrm{d}k}{\mathrm{d}\sigma} + 0.466\frac{\mathrm{d}\theta}{\mathrm{d}\sigma} \tag{21}$$

for n=3
$$\frac{\mathrm{d}(\omega_3 / \omega_{3,0})^2}{\mathrm{d}\sigma} = \frac{1}{k_0}\frac{\mathrm{d}k}{\mathrm{d}\sigma} - 0.684\frac{\mathrm{d}\theta}{\mathrm{d}\sigma} < 0 \tag{22}$$

for n=4
$$\frac{\mathrm{d}(\omega_4 / \omega_{4,0})^2}{\mathrm{d}\sigma} = \frac{1}{k_0}\frac{\mathrm{d}k}{\mathrm{d}\sigma} + 0.3185\frac{\mathrm{d}\theta}{\mathrm{d}\sigma} \tag{23}$$

Finally, we can write for the c_{n1} in eq.(14-15):

$$c_{n1} = \frac{1}{k_0} \tag{24}$$

3 Conclusions

3.1 General behavior

Since always d*k*/dσ<0, namely

$$\frac{1}{k_0}\frac{\mathrm{d}k}{\mathrm{d}\sigma} = -\frac{0.784}{\sigma_{th}} \tag{25}$$

and dθ/dσ>0, it automatically follows that $\mathrm{d}\omega_1/\mathrm{d}\sigma<0$ for n=1 and n=3. This tells us that the related curve must decrease with increasing stress.

For n=2 and n=4 there are positive *and* negative contributions mixed. Only when the increase in dθ/dσ is strongly positive and overcompensates the negative *k*-influence, an increasing curve may be expected. This is obviously not the case in the measurements compiled in Figs.1 and 2. This implies that the effect of decreasing *k* is stronger than the increasing effect by θ. So far the increase of θ with increasing stress, dθ/dσ, is not exactly known.

3.2 Quantitative behavior for the stretching modes ASS and SS

The peak position for the SS and ASS-stretching modes under uniaxial tension σ_x (in GPa) were found by the measurements of Tallant et al. [2]. Since in eqs.(13-23) the squares of the relative peak positions, $(\omega/\omega_0)^2$, are used, we plotted the experimental results by Tallant et al. [2] in the same form in Fig. 5. The red symbols represent the data for the asymmetric stretching mode and the green ones the data for symmetric stretching. Straight-line fitting yields

$$(\omega/\omega_0)^2 = 1 + b\,\sigma \tag{26}$$

with the slope $b = -0.00487$ (1/GPa) for the ASS-mode and $b = -0.005704$ (1/GPa) for the SS-mode. These slopes are not strongly different.

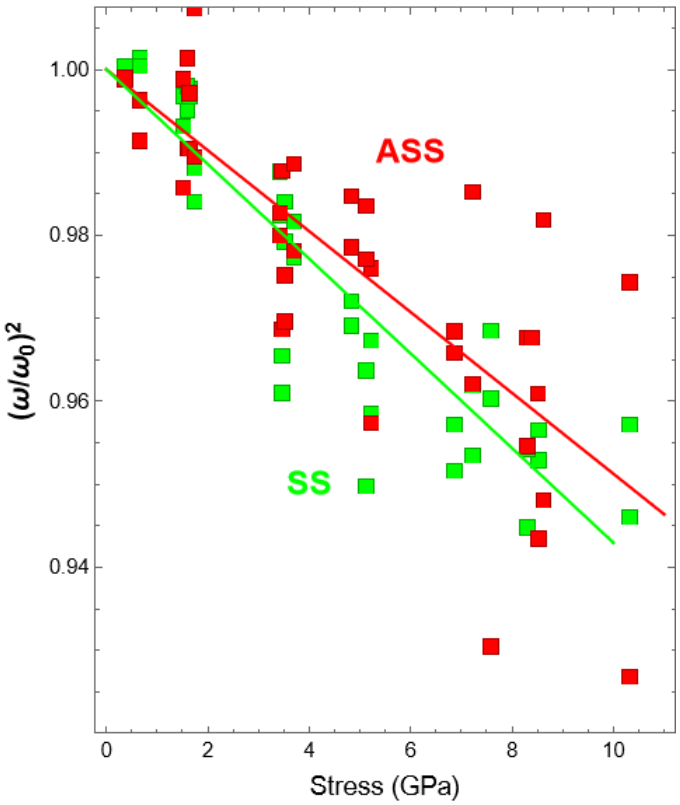

Fig. 5 Measurements of Raman-line position by Tallent et al. [2] in normalized form $(\omega/\omega_0)^2 = f(\sigma)$. Asymmetric stretching mode (ASS): red, Symmetric stretching mode (SS): green. Straight lines are obtained by least-squares fitting according to eq.(26).

In Fig. 6, all data are shown together, without distinguishing between ASS and SS. This total data base was fitted according to

$$(\omega/\omega_0)^2 = a + b\,\sigma \tag{27}$$

with the results a= 0.99988 [0.9942, 1.00557] and b= –0.00524 [-0.00628, -0.00420] (1/GPa), illustrated by the solid line. The numbers in brackets are the 99%-Confidence Intervals. The related limits are entered by the dashed lines.

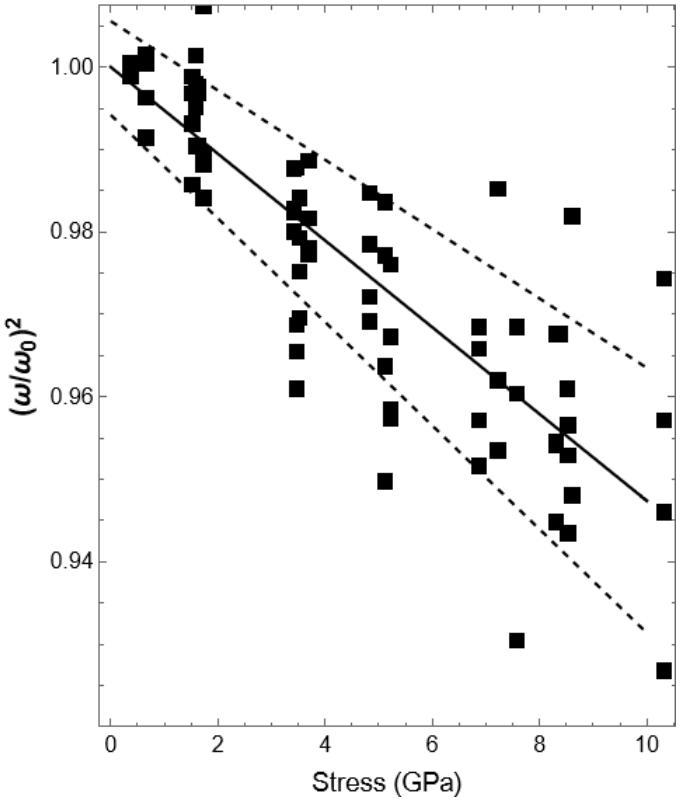

Fig. 6 Data by Tallant et al. [2] from Fig. 5 and fitting straight-line for all results (solid line). The dashed lines indicate the 99%-Confidence Interval.

Introducing eq.(27) into eq.(25) and assuming $d\theta/d\sigma \to 0$ gives for the estimate of the theoretical strength of the bond:

$$\sigma_{th} \cong \frac{-0.784}{-0.00628} = 125\ \text{GPa} \tag{28a}$$

and the ideal strength of the solid under uniaxial tension:

$$\sigma_0 = \tfrac{1}{3}\sigma_{th} \cong 41\ \text{GPa} \tag{28b}$$

The ideal strength σ_0 is higher than the measured value by Brambilla and Payne [12] on thin silica fibers of about 60 nm radius, resulting in $\sigma_0 \approx 25$ GPa.

References

1 F.L. Galeener, Band limits and the vibrational spectra of tetrahedral glasses, Phys. Rev. B, **19 (**1979), 4292-4297.

2 Tallant DR, Michalske TA, Smith WL. The effects of tensile stress on the Raman spectrum of silica glass, J. Non-Cryst Solids 106(1988), 380-82

3 P.N. Sen and M.F. Thorpe, Phonons in AX_2 glasses: From molecular to band-like modes, Rev. B **15** (1977), 4030 pp.

4 K. G. Schell, C. Bucharsky, S. Wagner, T. Fett, A contribution to stress-dependent vibration peaks - Asymmetric stretching mode - Uniaxial loading ,Scientific Working Papers SWP **250**, 2024, ISSN: 2194-1629, Karlsruhe, KIT.

5 Hemley R.J., Mao K.H., Bell P.M., Myssen B.O., Raman Spectroscopy of SiO_2 Glass at High Pressure, Physical Review Letters, **57**(1986), 747-750.

6 Vandembroucq D, Deschamps T, Coussa C, Perriot A, Barthel, Champagnon B, Martinet C, Density hardening plasticity and mechanical ageing of silica glass under pressure: a Raman spectroscopic study, HAL 2008, hal-00258599v1.

7 Deschamps T, Martinet C, de Ligny D, Champagnon B, Silica under hydrostatic pressure: A non continuous medium behavior, J. Non-Cryst Solids **355**(2009), 1095-1098.

8 M. Tomozawa, Y.-K. Lee, Y.-L. Peng, Effect of uniaxial stresses on silica glass structure investigated by IR spectroscopy, Journal of Non-Crystalline Solids **242** (1998), 104-109.

9 R.A.B. Devine, Ion implantation- and radiation-induced structural modifications in amorphous SiO_2, Journal of Non-Crystalline Solids **152** (1993) 50-58.

10 M. Tomozawa, Fracture of glasses, Annu. Rev. Mater. Sci. 1996. **26**:43-74

11 K. G. Schell, C. Bucharsky, S. Wagner, T. Fett, Stress-dependent vibration peaks in glass - Literature results, Scientific Working Papers SWP **253**, 2024, ISSN: 2194-1629, Karlsruhe, KIT.

12 G. Brambilla, D.N. Payne, The ultimate strength of glass silica nanowires, Nano Letters, **9**(2009), 831-835.

KIT Scientific Working Papers
ISSN 2194-1629

www.kit.edu